Research Square

Preprints are preliminary reports that have not undergone peer review.
They should not be considered conclusive, used to inform clinical practice,
or referenced by the media as validated information.

First-Principles Investigation of Nitrogen-Doped Layered MoSe2 for Exhaled Volatile Organic Compound Sensing towards Early Lung Cancer Detection

Tanvir Reza Niloy
Rajshahi University of Engineering & Technology
Shadman Akif Rayen
Rajshahi University of Engineering & Technology
Md. Rahat Al Hassan
Rajshahi University of Engineering & Technology
Naim Ferdous
naim.ferdous.badhan@gstu.edu.bd
Gopalganj Science and Technology University
Jewel Hossen
Rajshahi University of Engineering & Technology

Research Article

Keywords: Nitrogen-doped MoSe2 monolayer, Density Functional Theory, exhaled-breath sensing, Volatile Organic Compounds, lung cancer biomarker, TMDs

Posted Date: October 30th, 2026

DOI: https://doi.org/10.21203/rs.3.rs-11310698/v1

License: This work is licensed under a Creative Commons Attribution 4.0 International License.
Read Full License

Additional Declarations: No competing interests reported.

First-Principles Investigation of Nitrogen-Doped Layered $MoSe_2$ for Exhaled Volatile Organic Compound Sensing towards Early Lung Cancer Detection

Tanvir Reza Niloy[a], Shadman Akif Rayen[a], Md. Rahat Al Hassan[a], Naim Ferdous[b,*], Jewel Hossen[c]

[a]*Department of Ceramic & Metallurgical Engineering, Rajshahi University of Engineering & Technology, Rajshahi-6204, Bangladesh.*

[b]*Department of Electrical and Electronic Engineering, Gopalganj Science and Technology University, Gopalganj-8105, Bangladesh*

[c]*Department of Chemistry, Rajshahi University of Engineering & Technology, Rajshahi-6204, Bangladesh.*

*Corresponding author. Email: naim.ferdous.badhan@gstu.edu.bd

Abstract

Early, non-invasive lung-cancer screening based on exhaled volatile organic compounds (VOCs) has motivated the development of sensitive and selective two-dimensional gas-sensing materials. Herein, spin-polarized density functional theory calculations were employed to investigate Nitrogen-doped layered $MoSe_2$ (N- $MoSe_2$) as a candidate sensing material for three representative exhaled VOCs associated with lung cancer—benzene (C_6H_6), acetone (C_3H_6O), and isoprene (C_5H_8), benchmarked against pristine $MoSe_2$ monolayer. Nitrogen incorporation substantially enhanced the adsorption of all three VOCs, with adsorption energies changing from −0.41, −0.76, and −1.29 eV on pristine $MoSe_2$ to −0.61, −1.25, and −2.05 eV on N- $MoSe_2$ for C_6H_6, C_3H_6O, and C_5H_8, respectively. Hirshfeld analysis attributed this to a localized negative charge on the N dopant (−0.234 to −0.264 e) rather than large charge transfer. N-doping introduced a Fermi-level impurity state, narrowing the band gap from 1.55 to 0.57 eV, and raised sensitivity to 88.09–94.50% versus 82.46–85.54% for pristine $MoSe_2$. Recovery-time analysis indicated comparatively rapid desorption of benzene/acetone but strong isoprene chemisorption, reversible via UV/thermal treatment (400–500 K). These results identify N-$MoSe_2$ as a promising theoretical candidate for exhaled-VOC sensing and provide a basis for subsequent experimental assessment of its suitability for breath-based lung-cancer screening.

Keywords: Nitrogen-doped $MoSe_2$ monolayer; Density Functional Theory; exhaled-breath sensing; Volatile Organic Compounds; lung cancer biomarker; TMDs

1. Introduction

Lung cancer remains one of the most-deadly cancers worldwide, ranking as the second most prevalent cancer in both men and women and accounting for the highest mortality rate among all cancer types[1,2]. Current diagnostic methods include blood tests, chest X-rays, computed tomography (CT), magnetic resonance imaging (MRI), and positron emission tomography (PET) can establish the existence and staging of disease[3–5]. Furthermore, it is unfortunate to point out that this cancer is typically discovered at an advanced stage, which results in a low survival rate. In order to improve overall survival, it is crucial to find a new, sensitive, and quick way to detect lung cancer in its infancy and do curative surgery as soon as practical[6]. Researchers recently became aware of a novel approach that utilizes the identification of volatile organic compounds (VOCs), which can be detected in blood samples, exhaled breath, or the headspace of cancer cells[7–9]. It has been observed that certain molecules produced by developing tumors in the body release volatile organic compounds (VOCs) into the bloodstream and exchange with them in the lungs. Additionally, compared to healthy people, lung cancer patients have far greater quantities of volatile organic compounds (VOCs) in their exhaled breath, which makes it possible to identify potential lung cancer patients and evaluate the severity of those who have been diagnosed[10]. VOCs in exhaled breath, particularly alkanes and benzene derivatives, serve as established biomarkers for lung cancer. These include hydrocarbons such as isoprene (C_5H_8) and methyl cyclopentane (C_6H_{12}), hydrocarbon derivatives such as acetone (C_3H_6O), 2-propenal (C_3H_4O), and 1-propanol (C_3H_8O), and aromatic hydrocarbons such as benzene (C_6H_6), styrene (C_8H_8), and ethylbenzene (C_8H_9)[11–13].

Recently, many two-dimensional (2D) materials with elevated electron mobility and favorable chemical reactivity have been demonstrated to react strongly with gas molecules, including transition metal dichalcogenides (TMDs), III-IV compounds, and V group monolayers.[14,15]. The high surface-to-volume ratios and tunable electronic structures of the 2D materials can facilitate interactions with adsorbed molecular species. In particular, transition-metal dichalcogenides (TMDs), together with other atomically thin semiconductors, have been investigated extensively for gas adsorption and sensing. Defect engineering and chemical doping provide additional routes for modulating surface reactivity and electronic response. In this context, substitutional or defect-associated dopants can alter the local charge distribution and create chemically active sites, potentially improving the interaction between the sensing surface and target gas molecules.

Among the transition metal dichalcogenides (TMDs), the $MoSe_2$ monolayer has recently drawn a lot of interest for use in gas sensors because of its exceptional mechanical, optical, chemical, and physical properties. The $MoSe_2$ monolayer is composed of three atomic layers of Se−Mo−Se, with a band gap of 1.55 eV. The Mo atom is covalently bonded to six Se atoms to form a sandwiched material[16,17]. Despite these favorable characteristics, defect-free $MoSe_2$ is comparatively chemically inert, which can limit its interaction with target gas molecules. Recent studies have shown that incorporating defects and suitable metal dopants into $MoSe_2$ monolayers can substantially improve their chemical activity and sensing sensitivity.[18,19]. Besides, nitrogen (N) is a commonly employed dopant for the surface to enhance the material's sensing function because of its superior catalytic performance upon gas interactions[20]. Nitrogen is particularly attractive as a light-element dopant because incorporation on $MoSe_2$ can generate localized electronic states and modify the charge distribution at the surface, thereby providing potentially active adsorption sites.

In the present work, we investigate N-doped $MoSe_2$ monolayer as a candidate sensing material for selected exhaled-breath VOCs associated with lung cancer. The N-$MoSe_2$ model is constructed by introducing N atom at a Se site in the $MoSe_2$ monolayer. Benzene (C_6H_6), acetone (C_3H_6O), and isoprene (C_5H_8) are selected as representative target molecules, and their adsorption geometries, adsorption energies, charge redistribution, electronic structures, sensing

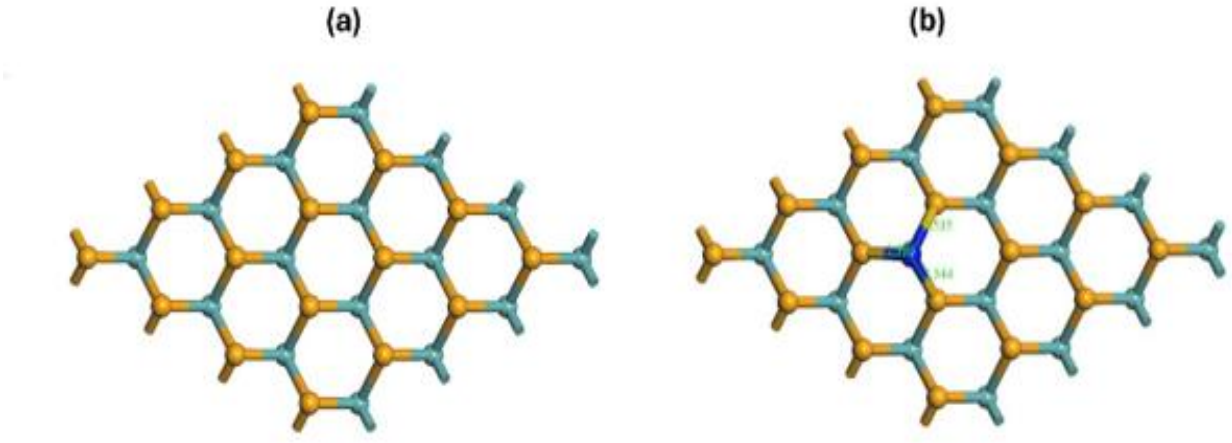


Figure 1: Optimized Structure of (a) $MoSe_2$ monolayer & (b) Nitrogen doped $MoSe_2$ (N-$MoSe_2$) monolayer

responses, and estimated recovery times are systematically compared with those of pristine $MoSe_2$. N doping substantially improves the adsorption capacity of $MoSe_2$ on VOCs. Our present work clarifies how nitrogen incorporation modifies the interaction between $MoSe_2$ and these VOCs and assess whether the resulting changes in electronic structure translate into

improved theoretical sensing characteristics. The results provide a computational basis for subsequent experimental investigations for breath-based lung cancer detection.

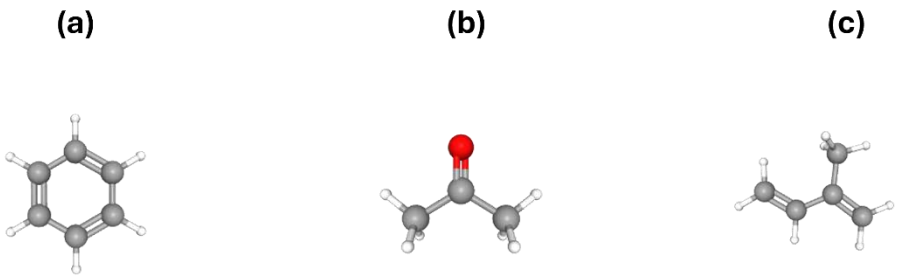


Figure 2: Geometric structure of three VOCs (a) C_6H_6, (b) C_3H_6O and (c) C_5H_8

2. Computational Details

The whole spin-polarized computations were performed with the DMol^3 package based on density functional theory (DFT) method[21]. The Perdew-Burke-Ernzerhof (PBE) function in the generalized gradient approximation (GGA) was employed to adjust for electron exchange correlation terms[22]. In terms of van der Waals force and long-range interactions, the Grimme method based on DFT-D2 was adopted[23]. Double numerical plus polarization (DNP) was selected as the atomic orbital basis set, and DFT semi-core pseudopotential (DSPP) method was selected to resolve the relativistic effect[24,25]. The Monkhorst-Pack grid's k-point sample was reduced to 5 × 5 × 1 of the Brillouin-zone for geometric optimization and electronic structure computations. We chose energy tolerance accuracy, maximum force, and displacement values of 10^{-5} Ha, 2×10^{-3} Ha/Å, and 5×10^{-3} Å, respectively. To accurately calculate total energy for static electronic structures, we used a 10^{-6} Ha self-consistent loop energy, a global orbital cut-off radius of 5.0 Å, and a smearing of 0.01 Ha[26,27]. A 4×4×1 $MoSe_2$ monolayer supercell comprising 16 Mo and 32 Se atoms was constructed with a 15Å vacuum layer along the out-of-plane direction to minimize spurious interactions between periodic images. The pristine supercell was subsequently fully relaxed to its energetically most stable configuration prior to the adsorption calculations.

3. Results & Discussion

3.1 Geometry optimization

Structural relaxation was performed at first to determine the equilibrium geometries of pristine and N-doped $MoSe_2$ layer and their VOC-adsorbed configurations. The optimized structures of the free standing $MoSe_2$ and N-$MoSe_2$ layers are illustrated in Figure 1 and 2, respectively;

while the $MoSe_2$ and N-$Mose_2$ layers with selective VOC gases benzene, acetone, isoprene are presented in Figure 3 and 4, respectively. The optimized N-$MoSe_2$ structure exhibits slight structural deformation compared with pristine $MoSe_2$.The bond lengths between the constituent atoms in the optimized structures of pristine $MoSe_2$, and N-$MoSe_2$ are presented in Table 1& 2, respectively. The obtained results indicate that gas adsorption causes a slight increase in the bond lengths of both $MoSe_2$ and N- $MoSe_2$, resulting in negligible structural deformation of the substrates.

Table 1: Average bond changes for gas adsorption on $MoSe_2$ monolayer

Bond	$MoSe_2$	$MoSe_2 + C_6H_6$	$MoSe_2 + C_3H_6O$	$MoSe_2 + C_5H_8$
Se-Mo	2.554	2.549	2.55	2.545
C-C		1.4	1.498	1.504
C-H		1.08	1.111	1.093
C=O			1.222	
Mo-C		3.34		3.676
Mo-O			3.61	
C=C				1.331

Table 2: Average bond length changes for gas adsorption on N-$MoSe_2$ monolayer

	N-$MoSe_2$	N-$MoSe_2 + C_6H_6$	N-$MoSe_2 + C_3H_6O$	N-$MoSe_2 + C_5H_8$
Se-Mo	2.585	2.551	2.57	2.551
N-Se	2.207	2.21	2.155	2.208
N-Mo	2.037	2.139	2.233	2.085
C-C		1.401	1.513	1.512
C=O			1.228	
C-H		1.092	1.120	1.095
C=C				1.334
Mo-C		3.45		3.85
Mo-O			3.63	

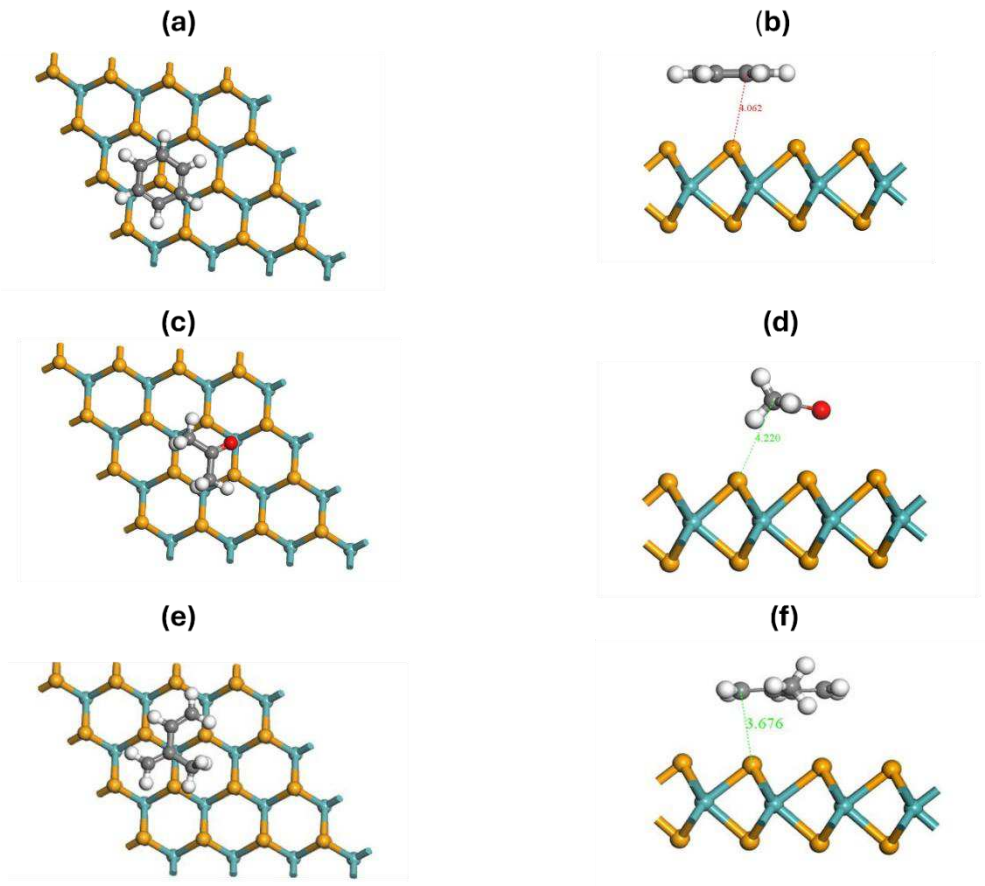


Figure 3: Optimized structures of (a) front and (b) edge view of $MoSe_2$ with benzene; (c) front and (d) edge view of $MoSe_2$ with acetone; (e) front and (f) edge view of $MoSe_2$ with isoprene.

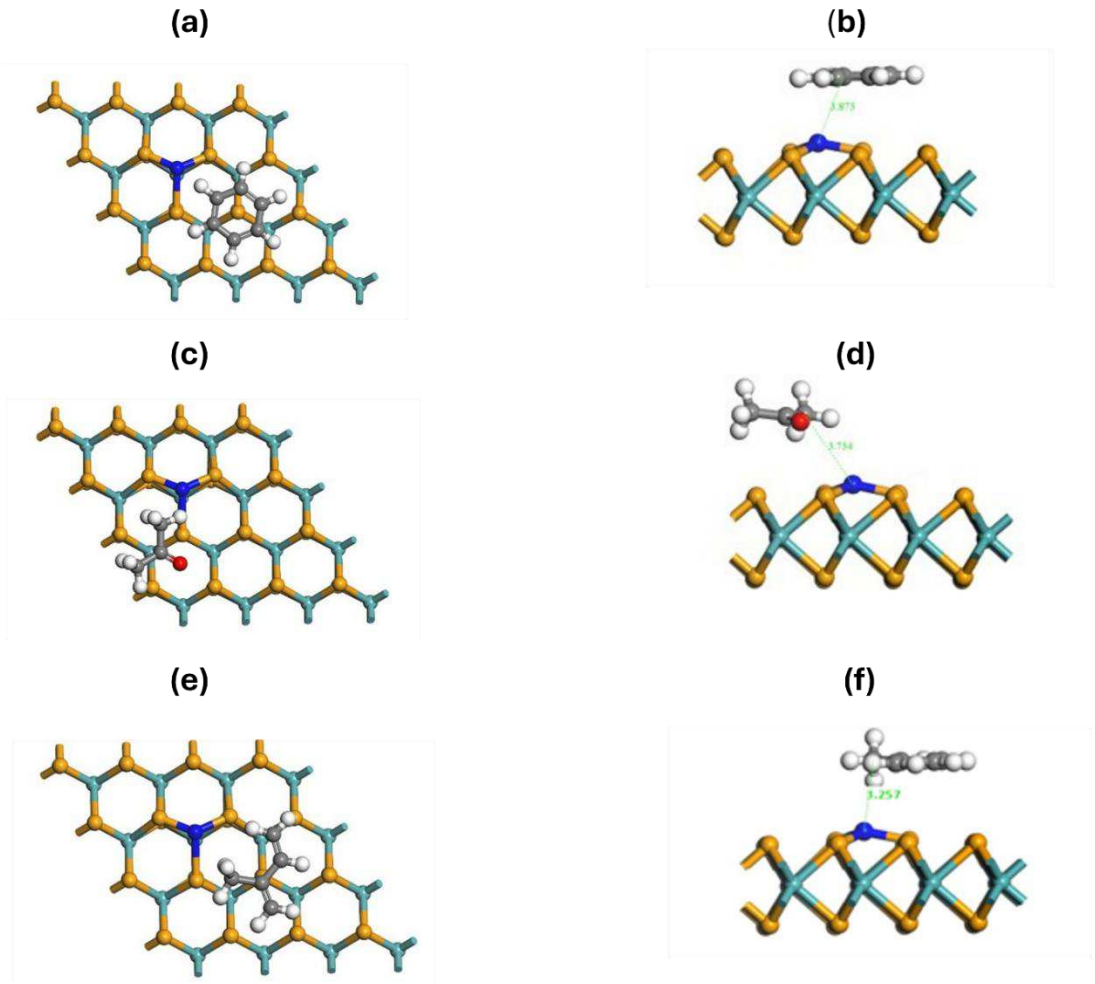


Figure 4: Optimized structures of (a) front and (b) edge view of N-$MoSe_2$ with benzene; (c) front and (d) edge view of N-$MoSe_2$ with acetone; (e) front and (f) edge view of N-$MoSe_2$ with isoprene.

3.2 Adsorption Performance Analysis

In the present work, we have calculated the adsorption energy for the C_6H_6, C_3H_6O, and C_5H_8 gas molecules on the monolayer by following equation[28]:

$$E_{Ads} = E_{monolayer+gas\ molecule} - E_{monolayer} - E_{gas\ molecules} \quad \text{.....(1)}$$

where, $E_{monolayer+gas\ molecule}$, $E_{monolayer}$ and $E_{gas\ molecules}$ are the energy of the complex, the energy of the $MoSe_2$ or N-$MoSe_2$ monolayer and the energy of the isolated gas molecules, respectively.

Table 3: Adsorption energy, Adsorption distance & Hirshfeld charge of gas molecules on $MoSe_2$ and N-$MoSe_2$ layer

Absorbed Gas	Adsorption energy(eV)		Adsorption distance(Å)		Hirshfeld Charges(e)		
	$MoSe_2$	N-$MoSe_2$	$MoSe_2$	N-$MoSe_2$	$MoSe_2$	N-$MoSe_2$	N
C_6H_6	-0.405	-0.61	4.062	3.873	-0.057	-0.075	-0.234
C_3H_6O	-0.76	-1.25	4.220	3.734	-0.089	-0.095	-0.261
C_5H_8	-1.29	-2.05	3.676	3.257	-0.079	-0.082	-0.264

When C_6H_6 is absorbed on the pristine $MoSe_2$ surface, the adsorption energy is -0.405 eV at an equilibrium distance of 4.062 Å, indicative of a weak physisorption-dominated interaction of van der Waals-type binding for aromatic ring on a 2D surface. After the N-doping, the adsorption energy is more negative to -0.614 eV and the adsorption distance is shortened to 3.873 Å. The interaction is moderately enhanced. The relatively small change can be attributed to the absence of strongly electron-donating or electron-withdrawing functional groups in benzene. Consequently, its interaction with the surface is governed primarily by the delocalized π-electron cloud, resulting in comparatively weak electronic perturbation. N doping slightly improves this π-surface interaction, but it stays weak, physical-type bonding rather than becoming a stronger chemical bond.

In terms of the C_3H_6O incorporated system, it binds more strongly than benzene, even on pristine $MoSe_2$. Its adsorption energy is -0.76 eV, at a distance of 4.220 Å. This is attributable to that, the molecule is polar and its dipole allows a better interaction with the surface. N-doping makes this binding much stronger. The adsorption energy is more negative to -1.25 eV, and the distance becomes shorter, at 3.734 Å. These changes suggest that the interaction is moving toward chemisorption, not just physisorption. This is likely caused by the oxygens lone pair donating electrons to the region near the N-dopant, which lacks electrons. In addition, C_5H_8 shows the strongest interaction of all three gases. On pristine $MoSe_2$, it binds with an energy of -1.29 eV at a distance of 3.676 Å. After N doping, the binding gets much stronger, dropping to -2.05 eV and the biggest gain among the three gases. N-doping strengthens C_5H_8 adsorption by causing local charge redistribution around the N dopant.

Hirshfeld charge analysis reveals that all three gas molecules acquire a small negative charge upon adsorption, with the net charge variation following N-doping limited to approximately 0.003-0.018 e. These results indicate that the enhanced adsorption strength cannot be attributed to substantial charge transfer between the doped surface and the adsorbed gas molecules. Instead, the N atom has a strong negative charge of -0.234 to -0.264 e. The nearby Mo and Se atoms show small changes in their charges. So, N-doping mainly changes the charge around the N atom. This change makes the gas molecules interact more strongly with the $MoSe_2$ surface. In summary, the adsorption of the N-$MoSe_2$ monolayer on the three VOCs is chemisorption, and the adsorption capacity is ranked as C_5H_8> C_3H_6O> C_6H_6. Compared with other studies on the adsorption of VOCs by gas sensing materials Table 4, the N-$MoSe_2$ monolayer proposed in this study has significant advantages in adsorption performance.

Table 4: Adsorption Performance of various gas sensor toward VOCs including this work

Gas Sensing material	Target Gas	Adsorption energy, E_{ad} (eV)
Al-$MoSe_2$ [29]	C_3H_4O	-1.45
	C_3H_6O	-1.80
	C_5H_8	-2.00
Ni-MoS_2 [30]	C_6H_6	-1.52
	C_3H_4O	-1.75
	C_5H_8	-1.84
N-$MoSe_2$ in this work	C_6H_6	-0.61
	C_3H_6O	-1.25
	C_5H_8	-2.05

3.3 Electronic Property Analysis

3.3.1 Band Structure Analysis

The band structures of pristine $MoSe_2$ and gas adsorbed systems C_6H_6, C_3H_6O & C_5H_8 are shown in Figure 5. The calculated band gap of pristine $MoSe_2$ is about 1.55 eV. The band gap of $MoSe_2$ changes only a little after gas adsorption. It decreases to 1.46 eV for both C_6H_6 and C_3H_6O, and to 1.45 eV for C_5H_8. This small change shows that the gas molecules have only a weak effect on the electronic structure of pristine $MoSe_2$. The nearly unchanged band shape also suggests a weak physisorption type interaction. Figure 6 shows the band structure of N-$MoSe_2$ before and after gas adsorption. The band gap decreases from 1.55 eV for pristine

$MoSe_2$ to 0.57 eV after N-doping. This large decrease is caused by the new electronic state introduced by the N atom near the fermi level. This state appears as an almost flat band in the band structure[31] . After the three gases are adsorbed on N-$MoSe_2$, the band gap decreases further. The values are 0.46 eV for C_6H_6, 0.45 eV for C_3H_6O, and 0.42 eV for C_5H_8. C_5H_8 shows the largest decrease of 0.15 compared with the N-MoSe2. In contrast to the order of E_{ad} (C_6H_6< C_3H_6O< C_5H_8), the rising order of the band gaps in the three systems is C_6H_6> C_3H_6O> C_5H_8.

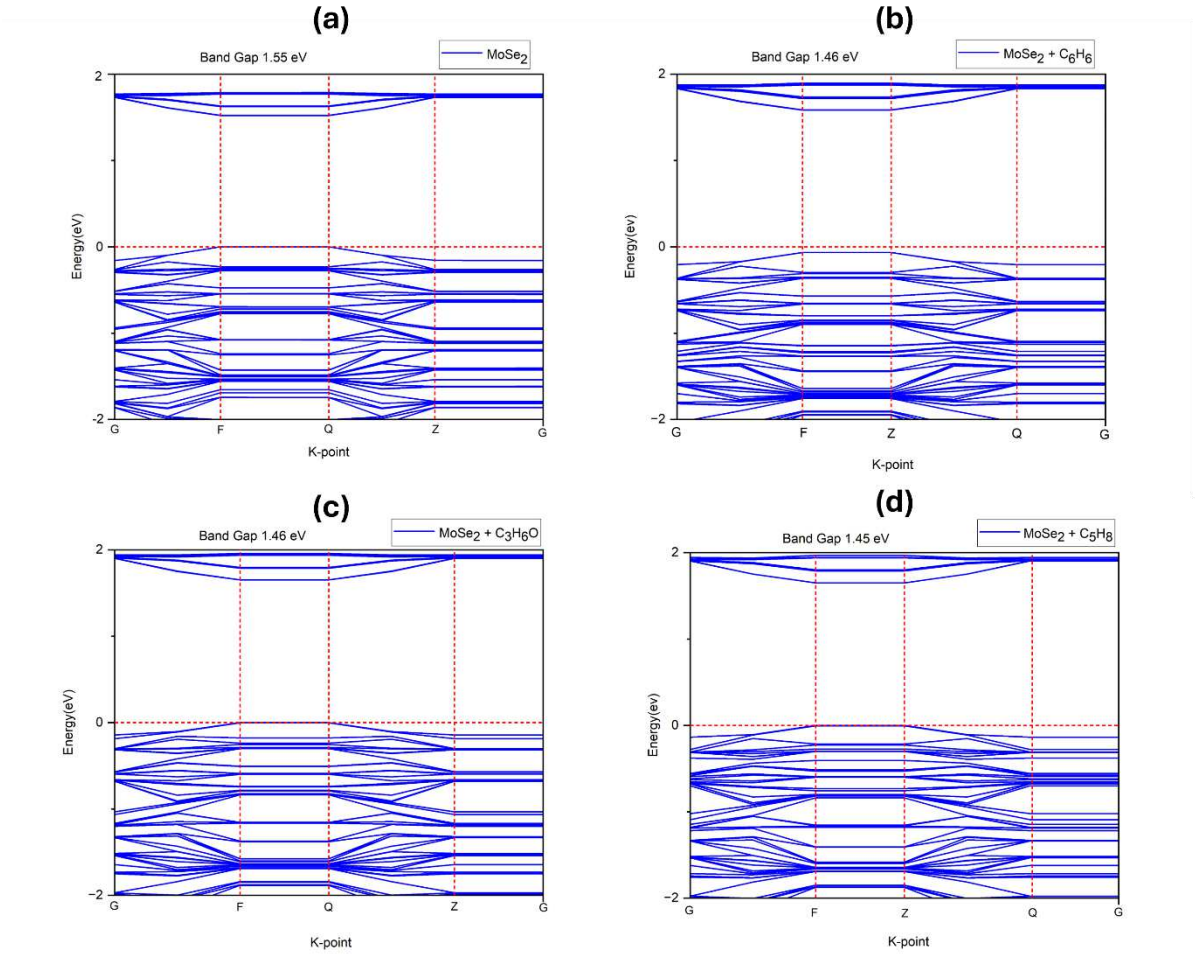


Figure 5: Band structures of (a) $MoSe_2$, (b) $MoSe_2$ + C_6H_6, (c) $MoSe_2$ + C_3H_6O, & (d) $MoSe_2$ + C_5H_8

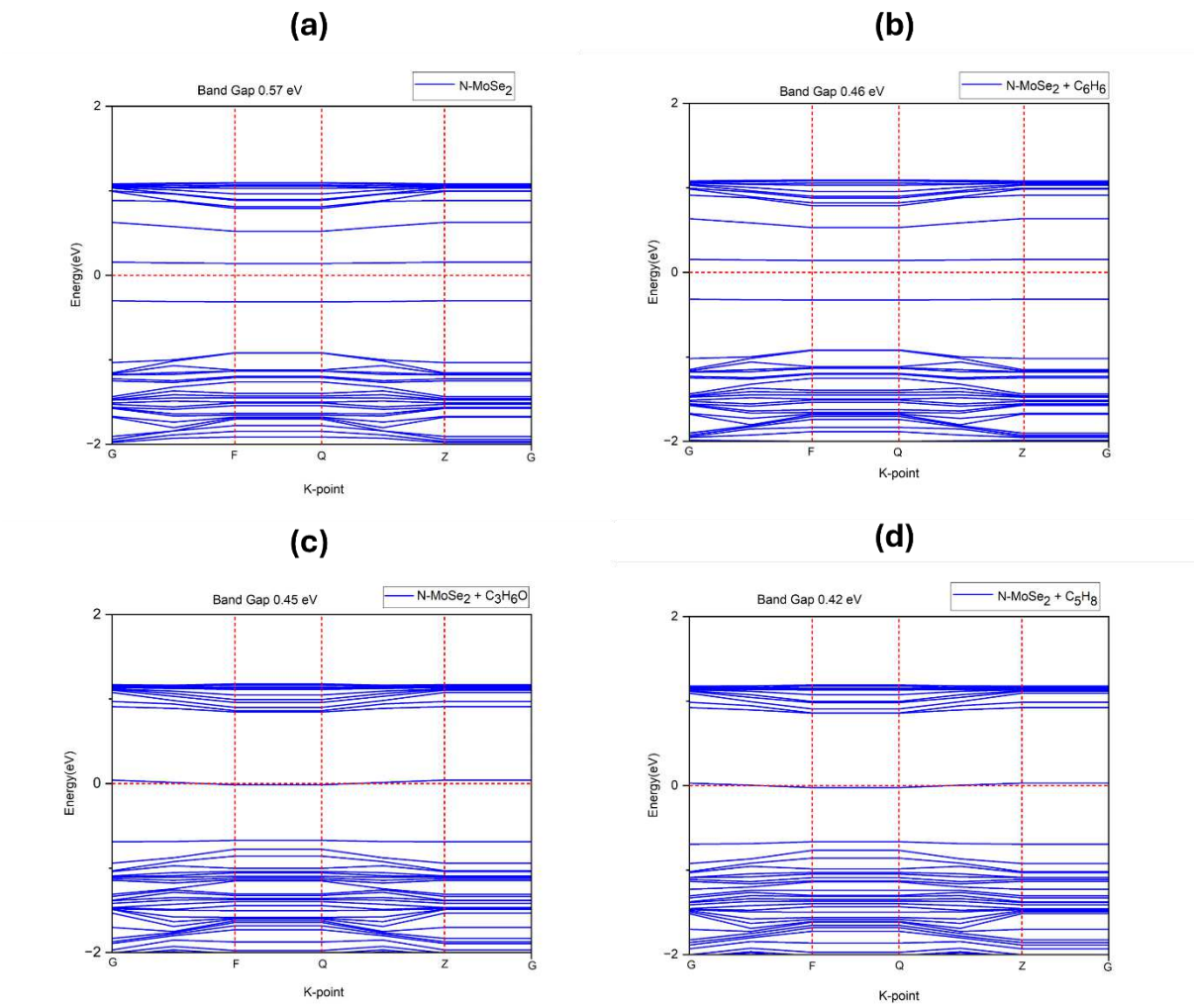


Figure 6: Band structures of (a) N-$MoSe_2$, (b) N-$MoSe_2$ + C_6H_6, (c) N-$MoSe_2$ + C_3H_6O, & (d) N-$MoSe_2$ + C_5H_8.

3.3.2 Density of States Analysis

The density of states (DOS) is the number of electronic states per unit volume per unit energy. It is useful for determining whether a material behaves as a metal, semiconductor or insulator [32]. If there are no electronic states at the Fermi level (E_f), then it indicates a presence of a band gap, which means that the material is either a semiconductor or insulator. In contrast, if electronic states are present at the Fermi level, there is no band gap, and the material shows metallic behavior[33]. Figure 7 presents the total density of states (TDOS) of $MoSe_2$ monolayer before and after the adsorption of selected gas molecules, while the TDOS of layered N-$MoSe_2$ before and after the adsorption of selected VOCs are illustrated in Figure 8.

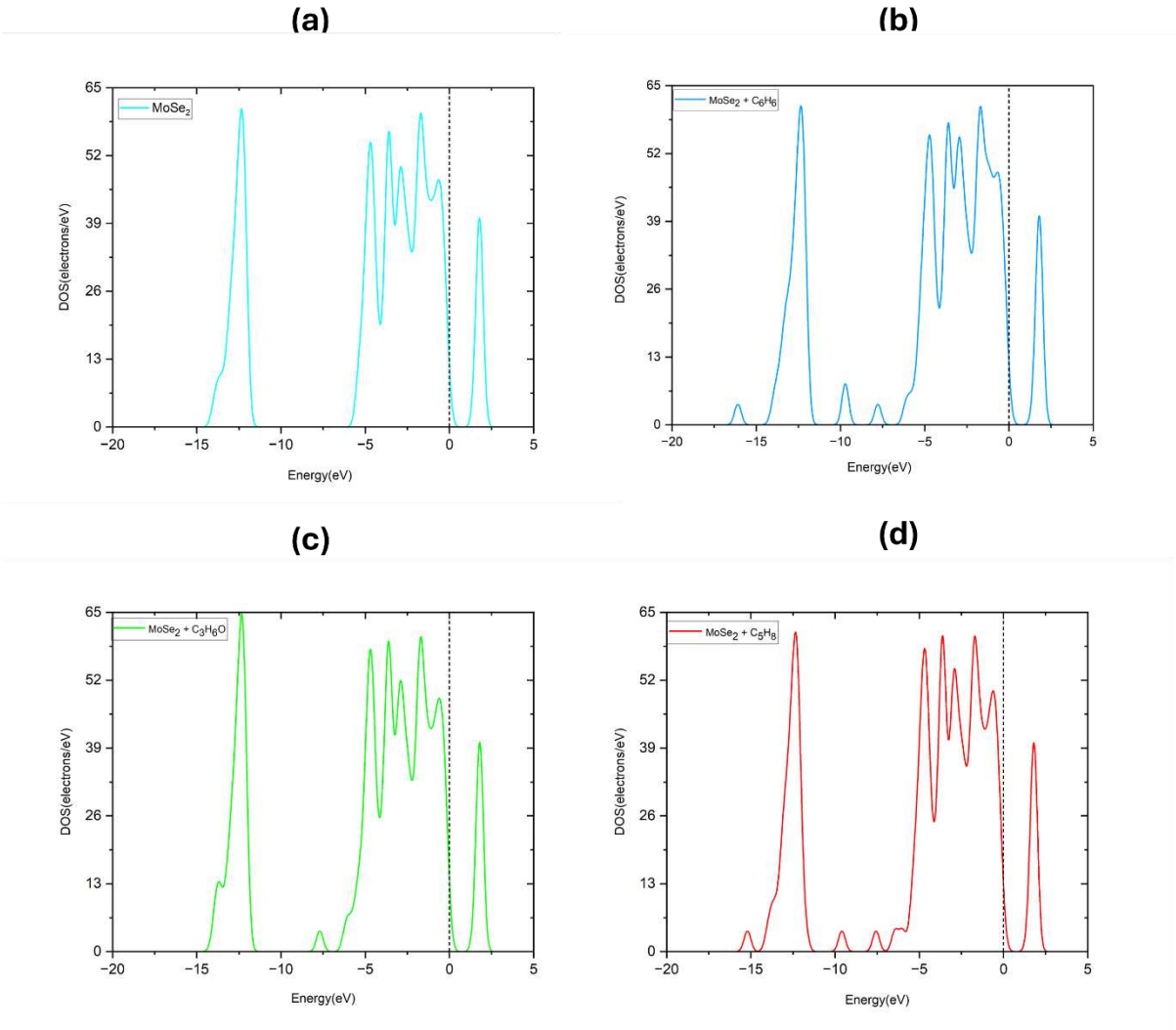


Figure 7: Total density of states (TDOS) of (a) $MoSe_2$, (b) $MoSe_2 + C_6H_6$, (c) $MoSe_2 + C_3H_6O$, & (d) $MoSe_2 + C_5H_8$

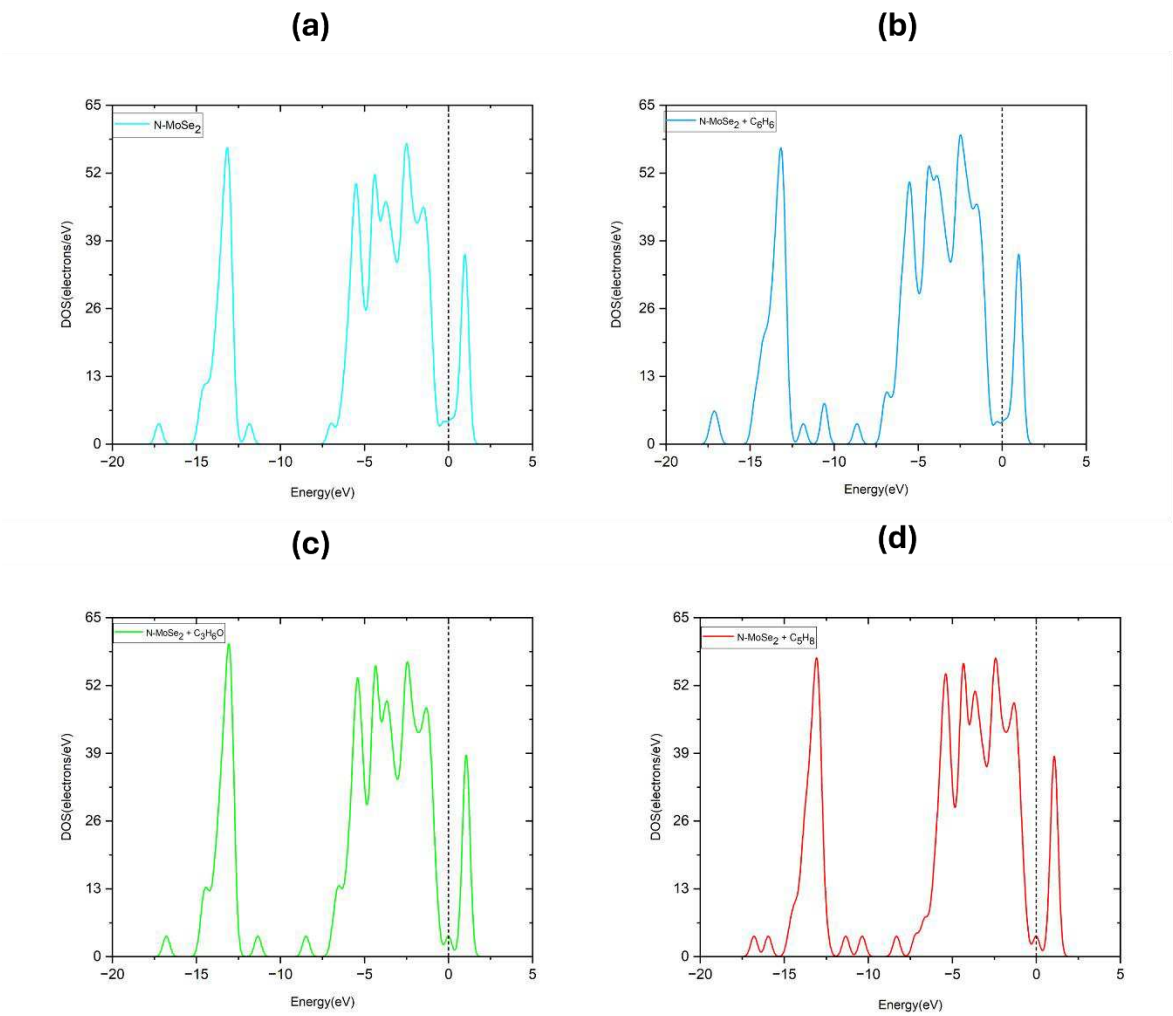


Figure 8: Total density of states (TDOS) of (a) N-$MoSe_2$, (b) N-$MoSe_2$ + C_6H_6, (c) N-$MoSe_2$ + C_3H_6O, & (d) N-$MoSe_2$ + C_5H_8

The DOS analysis is used to study the electronic changes in $MoSe_2$, after nitrogen doping and gas adsorption. Pristine $MoSe_2$ has a clear band gap. After nitrogen doping, a new state appears inside the band gap. This state is close to the Fermi level. It comes from the nitrogen atom. This new state makes the gap smaller. It also creates new active sites for reactions. When benzene, acetone, and isoprene are added to pure $MoSe_2$, the DOS does not change much. The band gap stays open. This means the gas molecules bind weakly. But when the same gases are added to N-doped $MoSe_2$, the new state near the Fermi level stays present. Only small changes happen in peak position and height. This shows that the doped surface keeps its high reactivity. It also keeps its sensitivity to these gases. These results show the nitrogen doping improves the electronic responses of $MoSe_2$.

3.4 Sensitivity Analysis

The resistance-type gas sensor's sensing mechanism may be determined based on the results found in Section 3.3.1. The sensitivity of a gas sensor depends on the change in band gap after gas adsorption. A smaller band gap gives higher electrical conductivity. So, a larger drop in band gap gives a higher sensitivity value. This can be done using the following formula[34–36] .

$$\sigma = \lambda . e^{(-\frac{B}{2kT})} \text{.....(2)}$$

$$S = \frac{\sigma^{-1}{}_{gas} - \sigma^{-1}{}_{pure}}{\sigma^{-1}{}_{pure}} = (\sigma_{pure} - \sigma_{gas})/\sigma_{gas} \text{.....(3)}$$

Where σ, λ, B_g, k, and T mean the electrical conductivity, certain constant, bandgap, Boltzmann constant, and working temperature in Equation 2, respectively. In Equation 3, σ_{gas} and σ_{pure} represent the conductivity of the adsorption system and $MoSe_2$ or N-$MoSe_2$ monolayer, respectively. For pristine $MoSe_2$, the sensitivity is 82.46% for C_6H_6, 82.46% for C_3H_6O, and 85.54% for C_5H_8. For N-$MoSe_2$, the sensitivity is 88.09% for C_6H_6, 90.18% for C_3H_6O, and 94.50% for C_5H_8. In both cases, the sensitivity shows the same order of C_5H_8> C_3H_6O> C_6H_6. This order matches the adsorption energy results. C_5H_8 has the strongest adsorption energy among the three gases. The N-doped surface gives higher sensitivity than the pristine surface for all three gases. This happens because N-doping already changes the charge distribution near the N atom. When a gas molecule come close, this charge distribution changes even more, This makes N-$MoSe_2$ a better material for detecting these VOCs. Figure **9** illustrates the bar chart of the sensitivity of $MoSe_2$ and N-$MoSe_2$ monolayer toward C_6H_6, C_3H_6O, and C_5H_8 gases at 300K temperature.

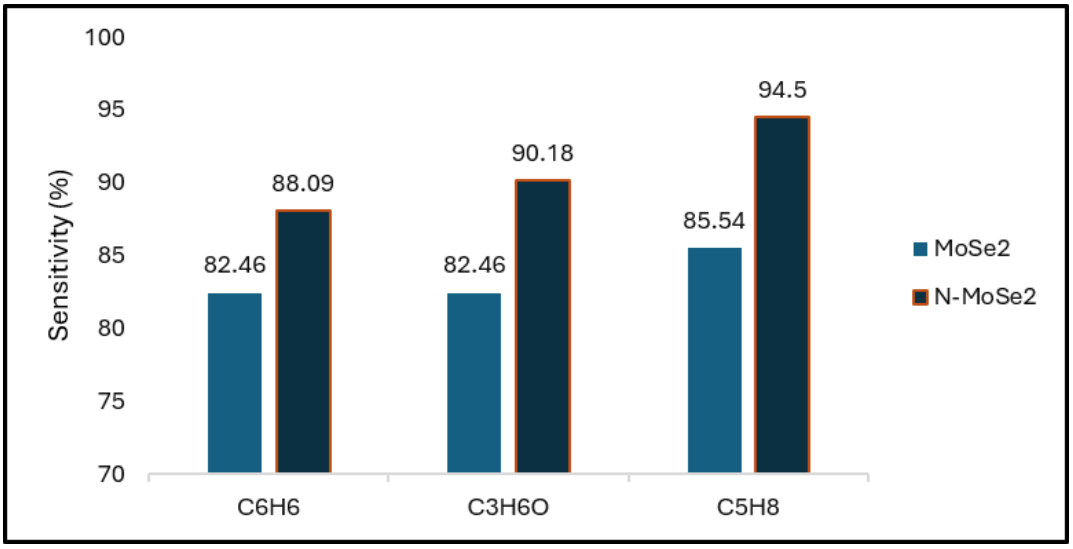


Figure 9: Sensitivity of pristine $MoSe_2$ and N-$MoSe_2$ monolayers toward C_6H_6, C_3H_6O, and C_5H_8 gas molecules at 300 K.

3.5 Recovery time Analysis

The recovery property, meanwhile, is another important parameter to evaluate the reusability of a chemical gas sensor. In order to achieve this, the van't-Hoff-Arrhenius method is used to define the recovery time (τ), which is the minimum time for the adsorbed gases to desorb from the N-$MoSe_2$ surface [37].

$$\tau = Ae^{\left(-\frac{E_a}{K_B T}\right)} \quad \text{.....(4)}$$

where A is the attempted frequency (10^{12} s^{-1}) [38], T is the temperature, and k_B is the Boltzmann constant (8.62×10^{-5} eV/K)). E_a is the potential barrier of desorption which in this work is determined to be equal to E_{ad}[39,40] . This formula suggests a relationship between the recovery time and the sensor's operating temperature.

Table 5: Calculated recovery time of C_6H_6, C_3H_6O, and C_5H_8 on pristine and N-doped $MoSe_2$ monolayers for both visible and ultraviolet light region situations.

Gas system	T=300K	T=400K	T=500K
$MoSe_2$+C_6H_6	6.33 µs	126.24 ns	12.05 ns
$MoSe_2$+C_3H_6O	5.80 s	3.74 ms	45.51 µs
$MoSe_2$+C_5H_8	146 years	4.72 hours	9.97 s
N-$MoSe_2$+C_6H_6	17.55 ms	48.23 µs	1.40 µs
N-$MoSe_2$+C_3H_6O	31.2 years	1.54 hours	3.94 s
N-$MoSe_2$+C_5H_8	8.5×10^{14} years	2.1×10^{6} years	14.4 years

Table 5 enlists the recovery time of the three VOCs on free-standing and N-doped $MoSe_2$ layers for both visible and ultra-violet light regions. At room temperature, the recovery time is very long for C_5H_8, especially on N-$MoSe_2$. This happens because N-doping makes the bond between the gas and the surface stronger. A stronger bond is hard to break. So, the gas stays on the surface for a very long time. UV light can help fix this problem, UV light gives extra energy, like raising the temperature. At 400k, the recovery time drops a lot for all the systems. At 500k, it drops even more. C_6H_6 and C_3H_6O recover in just seconds on both surfaces at 500k. But C_5H_8 on N-$MoSe_2$ still takes a long time to recover. This shows the main effect of N-doping clearly that the N-doping makes the sensor very sensitive to C_5H_8, but it also makes recovery harder.

4. Conclusion

In summary, we systematically investigated the adsorption and gas-sensing performance of N-doped monolayer $MoSe_2$ toward three representative exhaled-breath VOC biomarkers associated with lung cancer, namely benzene (C_6H_6), acetone (C_3H_6O), and isoprene (C_5H_8), using spin-polarized density functional theory. N-doping substantially enhances VOC adsorption, with adsorption energies of −0.61, −1.25, and −2.05 eV for C_6H_6, C_3H_6O, and C_5H_8, respectively, following the trend C_5H_8> C_3H_6O > C_6H_6. Hirshfeld charge analysis indicates that the enhanced adsorption originates from the modified local electronic environment induced by the negatively charged N dopant (−0.234 to −0.264 e), rather than from substantial charge transfer to the adsorbed molecules. N substitution also introduces an impurity state near the Fermi level and reduces the band gap from 1.55 to 0.57 eV, leading to enhanced electronic responses upon VOC adsorption. Accordingly, the calculated sensing responses of N-$MoSe_2$ toward C_6H_6, C_3H_6O, and C_5H_8 reach 88.09%, 90.18%, and 94.50%, respectively, exceeding those of pristine $MoSe_2$ (82.46%, 82.46%, and 85.54%). Moreover, benzene and acetone exhibit relatively favorable recovery at room temperature, whereas the strong chemisorption of isoprene results in prolonged recovery; this limitation can be substantially mitigated by UV illumination or elevated temperatures of 400–500 K. Collectively, these results demonstrate the potential of N-doped $MoSe_2$ as a two-dimensional sensing platform for exhaled-breath VOC detection and provide theoretical guidance for the experimental development of TMD-based sensors for breath analysis and related chemical-sensing applications.

Conflict of Interest:

The authors declare no conflict of interest.

Data availability:

All data supporting the findings of this work are available from the corresponding author upon reasonable request.

Funding sources:

This research did not receive grant from any funding agency.

Ethics, Consent to Participate, and Consent to Publish:

Not applicable. This study did not involve human participants, human data, or human biological samples.

Clinical Trial Registration:

Not applicable. This study was not a clinical trial.

References:

1. Z. Altintas and I. Tothill, Sens. Actuators B Chem. **188**, 988 (2013).
2. Z. Jia, A. Patra, V. K. Kutty, and T. Venkatesan, Metabolites **9**, (2019).
3. M. P. Lichy, P. Aschoff, C. Plathow, A. Stemmer, W. Horger, C. Mueller-Horvat, G. Steidle, M. Horger, J. Schafer, S. M. Eschmann, B. Kiefer, C. D. Claussen, C. Pfannenberg, and H. P. Schlemmer, Invest. Radiol. **42**, 605 (2007).
4. X. Chen, K. G. Muhammad, C. Madeeha, W. Fu, L. Xu, Y. Hu, J. Liu, K. Ying, L. Chen, and G. O. Yurievna, Lung Cancer **154**, 197 (2021).
5. J. Chung, S. Akter, S. Han, Y. Shin, T. G. Choi, I. Kang, and S. S. Kim, Int. J. Mol. Sci. **24**, (2023).
6. V. H. Tran, H. P. Chan, M. Thurston, P. Jackson, C. Lewis, D. Yates, G. Bell, and P. S. Thomas, IEEE Sens. J. **10**, 1514 (2010).
7. M. Hakim, Y. Y. Broza, O. Barash, N. Peled, M. Phillips, A. Amann, and H. Haick, Chem. Rev. **112**, 5949 (2012).
8. P. Wang, Q. Huang, S. Meng, T. Mu, Z. Liu, M. He, Q. Li, S. Zhao, S. Wang, and M. Qiu, EClinicalMedicine **47**, 101384 (2022).
9. P. Pisapia, F. Pepe, A. Baggi, M. Barberis, A. Galvano, V. Gristina, F. Mastrilli, S. Novello, F. Pagni, S. Pasini, G. Perrone, D. Righi, A. Russo, G. Troncone, and U. Malapelle, Crit. Rev. Oncol. Hematol. **169**, (2022).
10. M. Phillips, N. Altorki, J. H. M. Austin, R. B. Cameron, R. N. Cataneo, J. Greenberg, R. Kloss, R. A. Maxfield, M. I. Munawar, H. I. Pass, A. Rashid, W. N. Rom, and P. Schmitt, Cancer Biomarkers **3**, 95 (2007).
11. Q. Wan, Y. Xu, X. Chen, and H. Xiao, Mol. Phys. **116**, 2205 (2018).
12. T. Itoh, T. Nakashima, T. Akamatsu, N. Izu, and W. Shin, Sens. Actuators B Chem. **187**, 135 (2013).
13. Z. Jia, Y. Jiang, T. Shang, H. Cao, J. Li, L. Cong, P. Pu, H. Xu, Y. Liu, Y. Huang, D. Ma, J. Wu, R. Zhou, X. Wang, C. bao Han, and J. Liu, Journal of Nanobiotechnology **23**, (2025).
14. H. Cui, T. Liu, Y. Zhang, and X. Zhang, IEEE Sens. J. **19**, 5249 (2019).
15. C. Sun, L. Wang, W. Zhao, L. Xie, J. Wang, J. Li, B. Li, S. Liu, Z. Zhuang, and Q. Zhao, Adv. Funct. Mater. **32**, (2022).
16. C. Patra, V. K. Guna, S. Chakraborty, S. Mondal, and Y. Nandakishora, ACS Sens. **10**, 6347 (2025).
17. S. Y. Choi, Y. Kim, H. S. Chung, A. R. Kim, J. D. Kwon, J. Park, Y. L. Kim, S. H. Kwon, M. G. Hahm, and B. Cho, ACS Appl. Mater. Interfaces **9**, 3817 (2017).
18. S. R. Arnab, J. Haldar, and Md. S. Islam, (2024).
19. A. Mosahebfard and M. Moaddeli, J. Appl. Phys. **134**, (2023).
20. M. Khatun, M. H. Rocky, A. Al Roman, D. Roy, M. A. Badsha, and M. T. Ahmed, ChemistryOpen **14**, (2025).
21. B. Delley, Journal of Chemical Physics **113**, 7756 (2000).
22. H. Cui, X. Zhang, D. Chen, and J. Tang, Appl. Surf. Sci. **447**, 594 (2018).
23. A. Tkatchenko, R. A. DiStasio, M. Head-Gordon, and M. Scheffler, J. Chem. Phys. **131**, 094106 (2009).
24. D. Zhang, J. Wu, P. Li, and Y. Cao, J. Mater. Chem. A Mater. **5**, 20666 (2017).
25. B. Delley, Phys. Rev. B Condens. Matter Mater. Phys. **66**, 1 (2002).
26. Y. Wu, X. Wang, Y. Duan, and M. Peng, Philosophical Magazine (2022).
27. Y. Wu, D. Ding, Y. Wang, C. Zhou, H. Lu, and X. Zhang, Measurement (Lond). **190**, (2022).
28. S. Sun, J. Cao, Y. Zhang, J. Liu, and P. Jia, Inorg. Chem. Commun. **183**, (2026).

29. T. Liu, Z. Cui, X. Li, H. Cui, and Y. Liu, ACS Omega **6**, 988 (2021).
30. G. Zhao and M. Li, Appl. Phys. A Mater. Sci. Process. **124**, (2018).
31. J. Hwang, C. Zhang, Y. S. Kim, R. M. Wallace, and K. Cho, Sci. Rep. **10**, (2020).
32. A. Mottaghizadeh, Q. Yu, P. L. Lang, A. Zimmers, and H. Aubin, Phys. Rev. Lett. **112**, (2014).
33. M. I. Khan, M. I. Akber, M. Gul, N. Ul Ain, T. Iqbal, S. S. Alarfaji, and A. Mahmood, RSC Adv. **14**, 7040 (2024).
34. H. Cui, P. Jia, X. Peng, and P. Li, Mater. Chem. Phys. **249**, (2020).
35. X. Zhang, L. Yu, X. Wu, and W. Hu, Advanced Science **2**, (2015).
36. Y. Long, S. Y. Xia, L. Y. Guo, Y. Tan, and Z. Huang, Sensors **22**, (2022).
37. Y. Long, S. Y. Xia, L. Y. Guo, Y. Tan, and Z. Huang, Sensors **22**, (2022).
38. N. Mishra and B. P. Pandey, (2020).
39. Y. H. Zhang, Y. Bin Chen, K. G. Zhou, C. H. Liu, J. Zeng, H. L. Zhang, and Y. Peng, Nanotechnology **20**, (2009).
40. S. Peng, K. Cho, P. Qi, and H. Dai, Chem. Phys. Lett. **387**, 271 (2004).